



Randomness driven reentrant cluster glass behavior and unconventional electrical transport in Ti_2FeAl

Koushik P.  and K. Mukherjee 

School of Physical Sciences, Indian Institute of Technology, Mandi, Himachal Pradesh 175075, India



(Received 1 May 2024; revised 17 June 2024; accepted 8 August 2024; published 21 August 2024)

Reentrant glassy systems are a class of disordered magnetic materials which can potentially host noncollinear spin state. Here, we focus on the role of site disorder on emergence of reentrant cluster glass state and the underlying mechanism for observation of anomalies in electrical transport properties of Ti_2FeAl . Structural and magnetic studies of Ti_2FeAl (under our synthesis protocol) reveal that it hosts strong site disorder resulting in development of a reentrant cluster glass state (below 10 K) along with a ferromagnetic ordering (around 30 K). Electrical resistivity in this alloy mimics a Kondo-like behavior along with the presence of weak localization effect at low temperatures. Remarkably, Hall resistivity measurements in glassy regime indicate a nontrivial, unconventional contribution which is attributed to the existence of noncollinear spin state. We believe that our study offers an ideal platform to understand the influence of disorder on magnetic ground state of such ternary alloys.

DOI: [10.1103/PhysRevB.110.054433](https://doi.org/10.1103/PhysRevB.110.054433)

I. INTRODUCTION

The presence of structural disorder plays a pivotal role in shaping the physical properties of materials. It introduces complexities in the magnetic interactions, leading to intriguing phenomena such as spin-glass (SG) state, reentrant glassy state, and unconventional electrical transport properties. Understanding the interplay between disorder and magnetism is crucial for unraveling the exotic magnetic ground states and emergent phenomena observed in these materials. Among them, SGs are a family of chaotic magnetic materials that serve as important model systems for exploring complexity, frustration, and randomness [1]. SGs in general have vast number of ground states and complicated configuration space with valleys. The emergence of a SG state is usually due to site randomness, where the substitution of a small number of magnetic ions in a matrix of nonmagnetic ions leads to random distances between magnetic ions. This results in competing interactions in case of Ruderman-Kittel-Kasuya-Yosida (RKKY) type of exchange interaction, where the nature of interaction (ferromagnetic or antiferromagnetic) depends on distance between spins [2]. Another way to induce a SG state is through bond randomness. In a random-bond system, the nearest-neighbor interactions vary, leading to frustration. In certain cases, materials behave like an ordered magnet at higher temperatures but undergo a transformation to a glassy state upon cooling. These systems are identified as reentrant spin glass (RSG) and have garnered considerable interest in recent years because of their potential to host noncollinear spin state [3].

A promising class of materials in this context is full Heusler alloys (X_2YZ ; X and Y are transition elements and Z is a main group element belonging to *s*- and *p* blocks) [4]. They have a highly ordered $L2_1$ structure (Cu_2MnAl as the prototype; space group $Fm\bar{3}m$). In case of inverse Heusler alloys, the atomic number of X is smaller than that

of Y, and they crystallize in space group $F\bar{4}3m$ (XA structure, Hg_2CuTi as the prototype) [5]. Because of their ability to incorporate wide range of elements into their crystal structure, these alloys exhibit remarkable states like unconventional superconductivity [6], half metallicity [7], topological insulator [8], semimetallic states [9,10], skyrmions and antiskyrmions [11,12], etc. However, Heusler alloys (HAs) are prone to structural disorder resulting in deviation from their ideal structure, giving rise to realization of exotic states such as coexistence of Griffiths phase and RSG state [13], anomalous Hall effect in Co_2FeAl [14], disorder-driven non-Fermi liquid behavior [15], and disorder-induced weak localization effect, as noted in $\text{Co}_2\text{Fe}_{1-x}\text{Cr}_x\text{Si}$ [16]. Several Ti-based inverse HAs exhibit half metallicity and spin gapless semiconducting behavior [17–20]. However, the presence of structural disorder results in destruction of half metallicity [21]. Therefore, it is crucial to explore the physical properties of disordered systems. In this context, Ti_2FeAl is an interesting candidate. First-principle studies on this compound show that it adopts Hg_2CuTi -type structure and displays half-metallic ferro- (ferri)magnetism [22–24], whereas a combined theoretical and experimental investigation of physical properties of Ti_2FeAl revealed that the lowest energy of the unit cell is realized for $P4/mmm$ with a ferromagnetic (FM) state. Nevertheless, the Rietveld refinement gave the best result for primitive CsCl-type structure [25]. However, a recent first-principle study of this system indicates identical formation energy for both $L2_1$ and XA structure [26]. Also, an elaborated study on Al-Fe-Ti system indicates that Ti_2FeAl system is not a single disordered phase at low temperatures [27]. Hence, the above reports show a variety of possibilities for this system. Also, a comprehensive experimental study of physical properties of this alloy is lacking in literature. With this motivation we have investigated Ti_2FeAl in the following context: (i) to study the magnetic ground state and examine the possibility of evolution of novel magnetic phase at low temperature, and

(ii) to understand the impact of site disorder on the electrical transport mechanism.

Therefore, we have systematically studied the structural, magnetic, electrical transport, and thermodynamic properties of an arc-furnace cooled Ti_2FeAl . Our investigation reveals that this alloy crystallizes in cubic structure with random mixing of Ti, Fe, and Al atoms, leading to A2-type structural disorder. A FM ordering is noted around 30 K, followed by a reentrant cluster glass phase below 10 K. An up-turn in temperature dependence of resistivity and a negative magnetoresistance are noted below 40 K. Notably, a large unconventional contribution to Hall resistivity is noted in glassy regime, which points toward the existence of noncollinear spin state.

II. EXPERIMENTAL DETAILS

Polycrystalline ingot of Ti_2FeAl is prepared by arc melting the constituent elements (>99.99% purity), taken in stoichiometric amount in an arc furnace (Compact Arc Melter MAM-1 from Edmund Bühler) under an argon gas pressure of 0.7 bar. Also, to ensure homogeneity, the ingot is flipped over and remelted several times. We prepare 2 g of the sample and the weight loss after the final melting is found to be less than 1%. Here, we would like to mention that the arc-melted ingot is not subjected to any annealing; rather, it is rapidly cooled in the arc-furnace chamber to room temperature. The crystal structure and phase purity are confirmed by x-ray-diffraction (XRD) pattern obtained at room temperature (T) using Rigaku SmartLab x-ray diffractometer with Cu $K\alpha$ ($\lambda = 1.5406 \text{ \AA}$). The selected area electron diffraction (SAED) patterns are obtained using Tecnai G 2 20 S-Twin transmission electron microscope. Magnetic Property Measurement System, from Quantum Design, is used to perform T and magnetic field (H)-dependent dc and ac magnetization. T and H dependence of heat capacity (C) and resistivity (ρ) measurements are performed using the Physical Property Measurement System from Quantum Design. For resistivity measurements, sample is cut into rectangular piece and four-probe technique is employed.

III. RESULTS

A. Structural characterization

Room-temperature XRD pattern reveals that Ti_2FeAl prepared under our synthesis condition forms in single phase, without any trace of impurities or development of superstructure. We performed Rietveld refinement of the XRD data, considering XA-type crystal structure [Fig. 1(a)], using FULLPROF software [28]. However, the observed and calculated peak profiles do not match with each other since both (111) and (200) superlattice reflections are absent in the obtained XRD pattern. This is evident from Fig. 1(b). However, the calculated peak profile indicates the presence of peaks corresponding to these reflections [as denoted by asterisks (*) in Fig. 1(a)]. This points to the fact that Ti_2FeAl does not crystallize in XA-type structure. Similarly, attempts to refine using the $L2_1$ -type structure also fails in explaining the absence of (111) and (200) superlattice reflections. It has been suggested that HAs crystallize with considerable degree of antisite

TABLE I. Structural parameters obtained from the Rietveld refinement of x-ray-diffraction pattern obtained at 300 K. The data have been modeled with $Im\bar{3}m$ space group using FULLPROF suite software.

| Lattice constant [$a = b = c$ (Å)] | | | | 3.099 (4) | |
|-------------------------------------|---------|-----|-----|------------|-----------|
| Reduced χ^2 | | | | ~ 1.3 | |
| Atom | Wyckoff | x | y | z | Occupancy |
| Ti | $2a$ | 0 | 0 | 0 | 0.50 |
| Fe | $2a$ | 0 | 0 | 0 | 0.25 |
| Al | $2a$ | 0 | 0 | 0 | 0.25 |

disorder. Generally, this can be assessed by examining the intensity of ordering-dependent (111) and (200) superlattice reflections [29]. For Ti_2FeAl , the structure factor of (111) and (200) can be written as

$$F_{111} = 4[(f_{\text{Ti}_{4a}} - f_{\text{Fe}}) - i(f_{\text{Ti}_{4c}} - f_{\text{Al}})], \quad (1)$$

$$F_{200} = 4[(f_{\text{Ti}_{4a}} + f_{\text{Fe}}) - (f_{\text{Ti}_{4c}} + f_{\text{Al}})]. \quad (2)$$

From the above equations it can be inferred that the absence of superlattice reflections signifies the random mixing of Ti, Fe, and Al atoms, leading to A2-type disorder. In this case, all the Wyckoff positions become equivalent with a body-centered cubic (space group $Im\bar{3}m$). Rietveld refinement of the XRD pattern considering A2 disorder yields an excellent match between the observed and calculated peak profiles, as depicted in Fig. 1(c). Additionally, a powder XRD pattern simulated considering A2 disorder using VESTA [30] is shown in Fig. 1(d). The simulated pattern matches well with the observed pattern, confirming the presence of A2 disorder. This implies that even though Ti_2FeAl has theoretically been considered as a Heusler alloy, full and inverse Heusler structure are not realized in our case. This is also consistent with the observation of identical formation energy for both types of structure [26]. Therefore, we refer to this system as a body-centered cubic (bcc) alloy. The structural parameters obtained from Rietveld refinement are listed in Table I. Further, to confirm the absence of (111) and (200) reflections, we have indexed the SAED pattern obtained for Ti_2FeAl (spot size of $\sim 175 \text{ nm}$), as shown in Fig. 1(e). The observed concentric rings have been indexed with hkl values considering bcc structure (space group $Im\bar{3}m$), which are in good agreement with the inference drawn from the XRD studies. It is important to mention that the SAED pattern has been indexed considering the space group $Im\bar{3}m$ rather than the XA structure. If we had considered the XA structure, the four concentric rings would have corresponded to (220), (400), (422), and (440), respectively. This proves the absence of XA structure and confirms the presence of A2 disorder.

Additionally, to investigate the impact of T on lattice parameters, we collected T -dependent XRD patterns in the range of 10 to 300 K. The variation of lattice constant with T is shown in Fig. 1(f). It is noted that no significant changes are observed in the measured range. Here, we would also like to mention that the presence of A2 disorder significantly influences the magnetic ground state. In our case, when

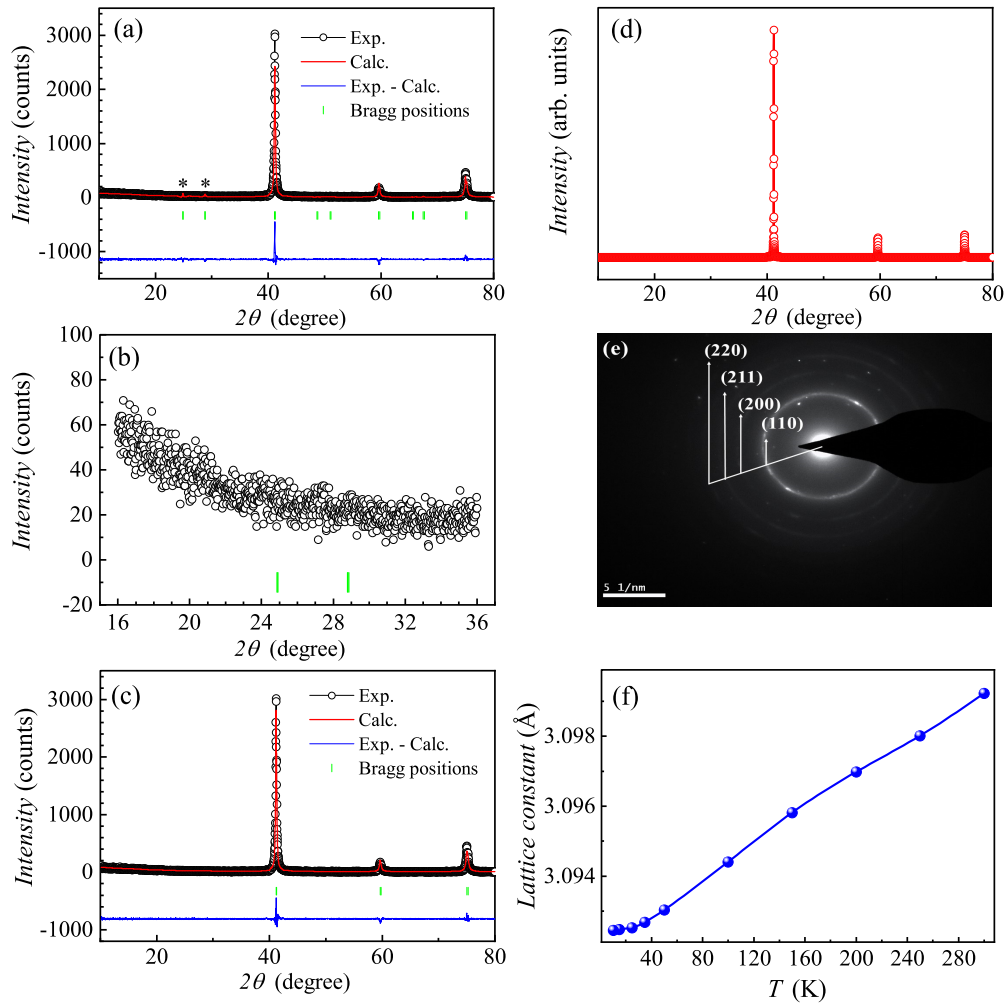


FIG. 1. (a) Rietveld refinement of XRD pattern of Ti_2FeAl considering XA structure. Asterisks (*) denote the presence of (111) and (200) reflections in calculated peak profile. (b) XRD pattern in 2θ range 16° – 36° . (c) Rietveld refinement of XRD pattern of Ti_2FeAl considering A2-type disorder. (d) The simulated powder XRD pattern with A2-type disorder using VESTA. (e) Indexed selected area electron diffraction (SAED) pattern taken at the scale 5 nm^{-1} . (f) Temperature dependence of lattice constant in the range 10–300 K.

crystallographically averaged, it is reasonable to assume that the chemical disorder in our system results in a random mixing of constituent elements. Hence, it may be visualized as a matrix where Fe atoms are randomly distributed. The nearest Fe atoms swap positions with nonmagnetic atoms, resulting in another nearest-neighbor interaction. Also, the mixing of atoms in the lattice results in random distances between Fe atoms. Generally, for such metallic alloys the magnetic exchange interactions are of RKKY type, which leads to the development of competing exchange interactions, resulting in a distorted spin arrangement at lower temperatures.

B. dc and ac magnetization

Temperature-dependent dc magnetic susceptibility (χ_{dc}) is measured under zero-field cooled (ZFC) and field-cooled (FC) protocols at 100 Oe and is shown Fig. 2(a). From the figure it is noted that χ_{dc} increases as T is lowered. A significant rise in χ_{dc} is observed upon cooling below 40 K in both ZFC and FC conditions. With further decrement in T , a broad hump is noted. Further, the χ_{dc} curves in both ZFC and FC conditions

follow the same path down to 6 K, below which a bifurcation is observed. This phenomenon typically arises from short-range correlations or a glassy magnetic state [31–33]. Further, T dependence of ac susceptibility (with an ac amplitude of 2 Oe) at 31 Hz is measured at zero applied dc field. Figure 2(b) represents the T dependence of real part of ac susceptibility (χ'). As seen from the figure, a steep increment in χ' is noted around 30 K, which is followed by a plateau down to 13 K. This points toward the presence of a FM ordering around 30 K. Upon further cooling, a sudden decrease in the value of χ' is observed, which is unusual in case of conventional ferromagnets. Here, it is important to note that the observed trend holds good only for this alloy prepared under our synthesis protocol.

Coming back to the Fig. 2(a), in analogy with χ' , it is observed that below 16 K, a decrement in the value of χ_{dc} is noted. This behavior points toward the development of a disordered magnetic state. Also, a weak shoulder is observed around 6 K [denoted by T^* in Fig. 2(a)]. Further, χ_{dc} measurements are carried out under different applied H . As seen from Fig. 2(c) (selected χ_{dc} plots are shown), with increasing

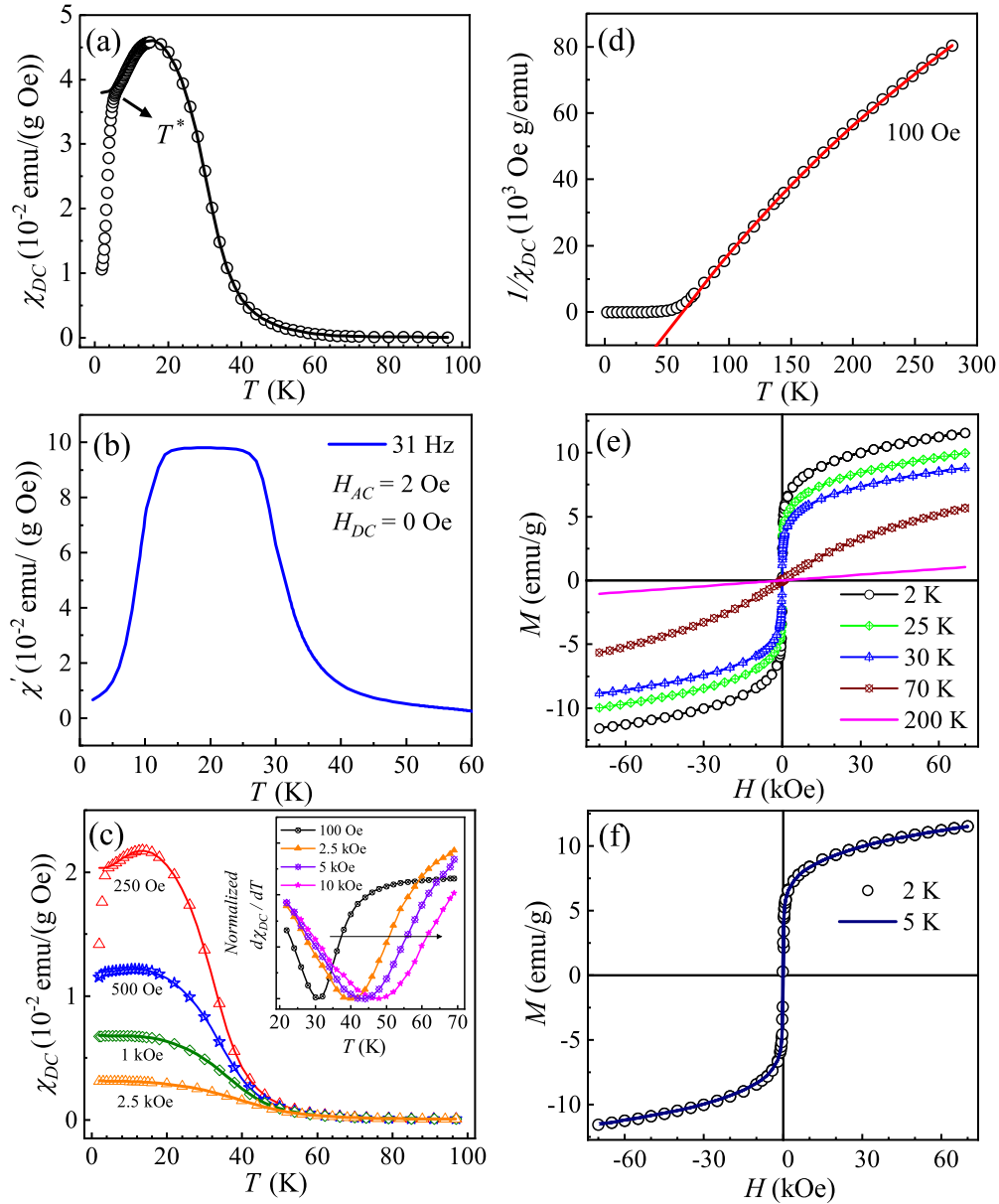


FIG. 2. (a) dc magnetic susceptibility (χ_{dc}) measured as function of temperature at 100 Oe in the temperature range 2 – 100 K. Open symbols and solid lines represent χ_{dc} measured in ZFC and FC protocols, respectively. (b) Temperature dependence of real part of the ac magnetic susceptibility (χ') in temperature range 2 – 60 K. (c) χ_{dc} measured as function of temperature at various applied fields in the temperature range 2 – 100 K. (d) Inverse dc susceptibility as a function of temperature at 100-Oe range 2–300 K. The red solid line corresponds to modified CW fit. (e) Magnetic isotherms as a function of magnetic field, measured at various temperatures in the range –70 to 70 kOe. (f) Magnetic isotherms measured at 2 and 5 K in the range –70 to 70 kOe.

H the absolute value of χ_{dc} decreases systematically, and the shoulder at T^* is suppressed towards lower T and vanishes at 1 kOe. Such behavior can be associated with antiferromagnetic interactions. Also, the bifurcation observed between the ZFC and FC curves is suppressed towards lower T with increment in H and it disappears as the field is increased beyond 10 kOe. This suggests the presence of a glassy magnetic phase at low T [1]. In order to confirm the nature of transition around 30 K, the temperature derivative of χ_{dc} at various H are plotted in the range 2–70 K, as shown in inset of Fig. 2(c) (selected normalized $d\chi_{dc}/dT$ plots are shown). The $d\chi_{dc}/dT$ curve at 100 Oe exhibits a prominent dip around 30 K. With increment

in H this dip broadens and shifts towards higher T . This is usually observed in case of ferromagnets and hence it can be said that Ti_2FeAl orders ferromagnetically around 30 K (T_c).

In order to determine the nature of dominating exchange interactions, the T response of inverse dc magnetic susceptibility (χ_{dc}^{-1}) is plotted at 100 Oe, as shown in Fig. 2(d). The curve is analysed using modified Curie-Weiss (CW) law:

$$\chi_{dc} = \chi_0 + \frac{C}{T - \theta_{CW}}, \quad (3)$$

where the first term indicates the temperature-independent contribution to the magnetic susceptibility which arises from

the core diamagnetism and Van Vleck paramagnetism. The second term corresponds to the CW law, where C and θ_{CW} denote the Curie constant and CW temperature, respectively. The best fit, as shown by red solid line, yields the values as $\chi_0 \sim 3.62 \times 10^{-6}$ emu/g Oe, $C \sim 0.00199$ emu/g Oe K and $\theta_{CW} \sim 62.92$ K. According to the mean-field theory, θ_{CW} represents the sum of all the exchange couplings. Therefore, the positive value of θ_{CW} indicates the presence of dominant FM interactions in our system. Additionally, the effective magnetic moment calculated using the formula $\mu_{eff} = 2.83\sqrt{C} \mu_B$ is found to be $1.68 \mu_B/\text{f.u.}$ (formula units). This value matches very well with the value reported in literature [25].

In order to comprehend the nature of magnetic phases, isothermal magnetization $[M(H)]$ is measured at various T , as depicted in Fig. 2(e). Above 100 K, the $M(H)$ curves exhibit a linear behavior. However, as the T is reduced to 70 K, a deviation from linearity is noted. As T is further lowered to 30 K, the $M(H)$ curves exhibit FM-like behavior. Interestingly, no saturation is achieved even at an applied field of 70 kOe. Below 10 K, the $M(H)$ curves mostly remain unaltered, as shown in Fig. 2(f). This indicates that the magnetic structure below 10 K is robust. The total saturation moment at 2 K is estimated by extrapolating the $M(H)$ curve at 70 kOe to $H = 0$ Oe. The obtained value of $0.37 \mu_B/\text{f.u.}$ matches well with literature [25].

The dc magnetization studies suggest the presence of a glassy magnetic state at low temperatures. Hence, to shed some light on this, we have employed the ac susceptibility technique (with an ac amplitude of 2 Oe and frequency range 31–731 Hz), which is a sensitive probe for such magnetic state. T -dependent ac susceptibility measurements both under zero field and various dc superimposed fields are conducted. Figure 3(a) depicts the T response of real part of ac susceptibility (χ') at 0 Oe. In analogy with χ_{dc} , χ' increases below 40 K with decreasing T . It exhibits a plateau between 28 and 13 K. Upon further cooling, a sudden decrease in the value of χ' is observed. Along with this, imaginary part of ac susceptibility (χ'') is also plotted as a function of T . As seen from the inset of Fig. 3(a), χ'' exhibits a frequency-dependent peak around ~ 10 K. Here, we would like to mention that χ'' exhibits a peak around 30 K, in accordance with dissipative losses associated with magnetic domain formation in a FM system (not shown). The characteristic frequency dependence observed at ~ 10 K is a common feature observed in glassy magnetic systems [31,34,35]. Therefore, the observed feature is attributed to a glassy transition. The freezing temperature (T_f) is characterized using the Mydosh parameter (δT_f), which is given by [31]

$$\delta T_f = \frac{\Delta T_f}{T_f \Delta \log_{10} \nu}, \quad (4)$$

where ΔT_f is the difference between the peak T at the lowest and highest frequencies, and $\Delta \log_{10}(\nu) = \log_{10}(\nu_1) - \log_{10}(\nu_2)$, respectively. For glassy systems, the Mydosh parameter falls in the range 0.005–0.09 whereas it lies in the range 0.1–0.3 for the superparamagnetic state. For our system, δT_f is found to be 0.034 which is the range of values observed for cluster glass (CG) systems [36–38]. Further, the observed behavior is investigated using standard critical slowing-down

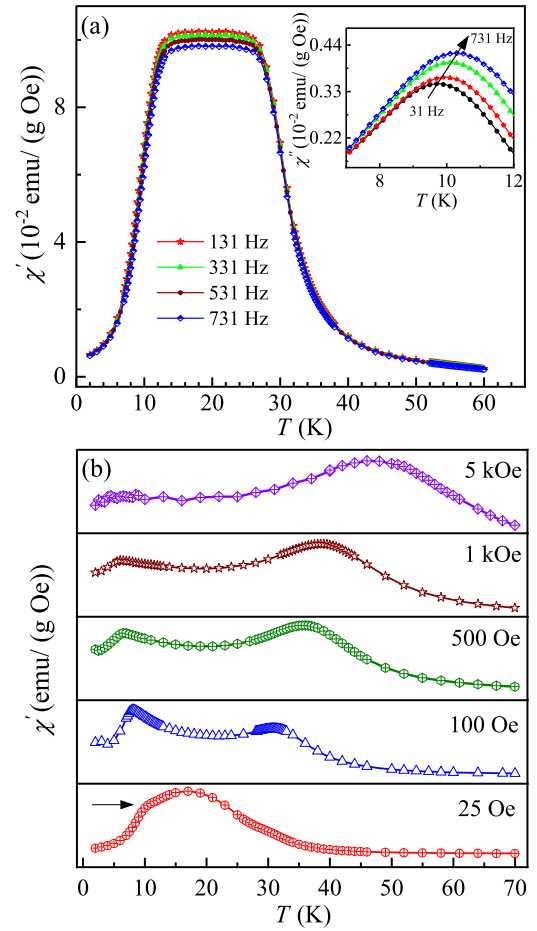


FIG. 3. (a) Temperature dependence of real part of the magnetic susceptibility (χ') measured at $H_{dc} = 0$ Oe and $H_{ac} = 2$ Oe in temperature range 2–60 K. Inset: The imaginary part of ac susceptibility in the range 7–12 K. The arrow indicates the shift of frequency-dependent peaks. (b) χ' measured at various dc fields in the temperature range 2–70 K.

model [31], given as

$$\tau = \tau^* \left(\frac{T_f - T_g}{T_g} \right)^{-z\nu}. \quad (5)$$

τ , τ^* , and T_g are the relaxation time corresponding to the excitation frequency, characteristic relaxation time for single spin flip, and freezing T when frequency approaches zero, respectively. $z\nu$ is a dynamical critical exponent which corresponds to the spin-spin correlation length (ξ), and is given as $\xi = [T_f/(T_g - 1)]^{-\nu}$ and $\tau \sim \xi^z$. The best fit to the equation is depicted in Fig. 4(a). The obtained value of τ^* is found to be around 9×10^{-7} s, which is large when compared to the typical values observed for canonical SG systems. This suggests slow spin dynamics arising due to interacting clusters in Ti_2FeAl . The value of T_g and $z\nu$ are found to be 9.70 ± 0.1 K and 2.08 ± 0.01 , respectively. Another dynamical scaling law, which takes into the account of interaction among the spins, phenomenological Vogel-Fulcher (VF) law of the form [39]

$$\tau = \tau_0 e^{\frac{E_0}{k_B(T_f - T_0)}}, \quad (6)$$

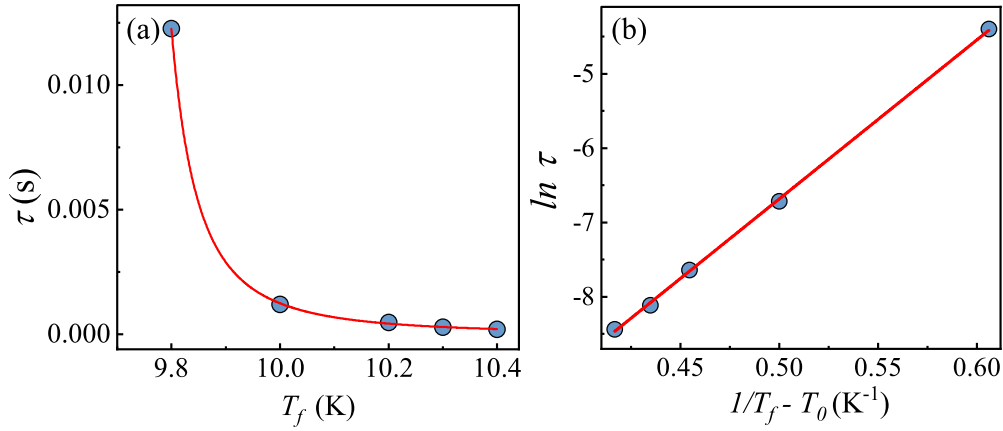


FIG. 4. (a) Plot of τ vs T_f and red solid line corresponds to critical slowing-down model. (b) Plot of $\ln \tau$ vs $1/T_f - T_0$. Red solid line shows the linear fit.

is also employed. Here, T_0 is the VF temperature, which is interpreted as the interaction strength among dynamic entities. Plot of $\ln \tau$ vs $1/(T_f - T_0)$ is shown in Fig. 4(b), which is fitted using Eq. (6). The obtained values of parameters τ_0 , T_0 , and E_a/k_B are 2.83×10^{-8} s, 8 ± 0.1 K, and 21.38 ± 0.2 K, respectively. The nonzero value of T_0 points towards the finite interaction among the spins. This further validates the presence of clusters in our system. Arrhenius law is applicable for noninteracting or very weakly interacting magnetic entities. It is given as

$$\tau = \tau_0 \exp\left(\frac{E_a}{k_B T}\right) \quad (7)$$

where τ_0 has the same physical meaning as τ^* , and E_a/k_B is the average activation energy [1]. The activation energy measures the energy barrier in which metastable states are separated. This law accounts for the timescale to overcome the energy barriers by activation process. The $\ln \tau$ vs $1/T_f$ data do not follow a linear behavior, suggesting the failure of Arrhenius law. This validates that the spin dynamics in our system is not due to single spin flip. Rather, it is a cooperative phenomenon due to intercluster interactions. From the above analysis it can be concluded that below 10 K, a CG phase is noted in Ti_2FeAl . Additionally, the observed glassy magnetic state is characterized by nonequilibrium dynamical and heat-capacity measurements, which are discussed in detail in Supplemental Material, Ref. [40], and Refs. [41–45].

Furthermore, ac susceptibility curves under various applied dc fields (at 31 Hz) are depicted in Fig. 3(b). At 25 Oe, χ' exhibits a weak shoulder around 10 K [as shown by an arrow in Fig. 3(b)]. With increasing H , this is suppressed towards low T and vanishes at 1 kOe. This is in analogy with analysis of χ_{dc} confirming the presence of weak antiferromagnetic correlations at low T . Further, it is noted that with increase in H , T_c and T_f separate from each other. The former transition shifts towards higher T , as expected for a FM transition, while the latter shifts towards lower T and is significantly suppressed upon the application of 5 kOe [as illustrated in the uppermost panel of Fig. 3(b)]. Hence, based on these observations, it can be concluded that this arc-furnace cooled Ti_2FeAl undergoes a FM ordering at 30 K followed by a transition to CG state at 10 K. Such transformation to a glassy state from an ordered

state is referred to as reentrant glassy transition [46,47]. Therefore, Ti_2FeAl is classified as a reentrant CG system. According to a theoretical model discussed by Nielsen *et al.*, it is believed that in site-disordered systems antiferromagnetic correlations develop due to swapping of magnetic ions with nonmagnetic atoms [48]. This introduces frustration, leading to a reduction in the average FM coupling within the system. At a threshold level of disorders, such systems exhibit a transition to glassy state. Further, the site disorders also result in few transversely placed spins which can give rise to a noncollinear state upon freezing [3,48,49]. It is important to note that the disorders do not disrupt the FM ordering around T_C . Here, in case of Ti_2FeAl , it is believed that the site disorders are at a threshold level, giving rise to emergence of a reentrant CG state at low T .

The presence of site disorders can substantially alter electrical transport properties. Additionally, the presence of noncollinear state in the glassy regime can give rise to an unconventional contribution to Hall effect. Therefore, we have performed electrical transport measurements.

C. Electrical resistivity and magnetoresistance

The temperature dependence of ρ is measured in the range of 2–300 K [as shown in Fig. 5(a)]. It is observed that ρ decreases with decrease in temperature down to 40 K, indicating a metallic behavior. As the T is further reduced, an upturn in ρ is noted below 40 K. This suggests the presence of additional scattering mechanisms, leading to a change in the sign of the temperature coefficient of resistivity. Such upturn in ρ curve has been reported in other disordered ternary alloys [50,51]. Therefore, the residual resistivity ratio (RRR) is calculated, which is found to be 1.08. The low value of RRR indicates the presence of significant disorder, which is consistent with the structural characterization of Ti_2FeAl .

Generally, the upturn in ρ is explained in terms of Kondo effect, electron-electron (e-e) interaction effect, or weak localization (WL) effect [52–54]. Kondo effect arises due to the scattering of conduction electrons by magnetic impurities. This results in a characteristic $\ln T$ dependence of ρ . Further, according to a theoretical prediction by Altshuler and Aronov, e-e interaction in presence of disorder induces

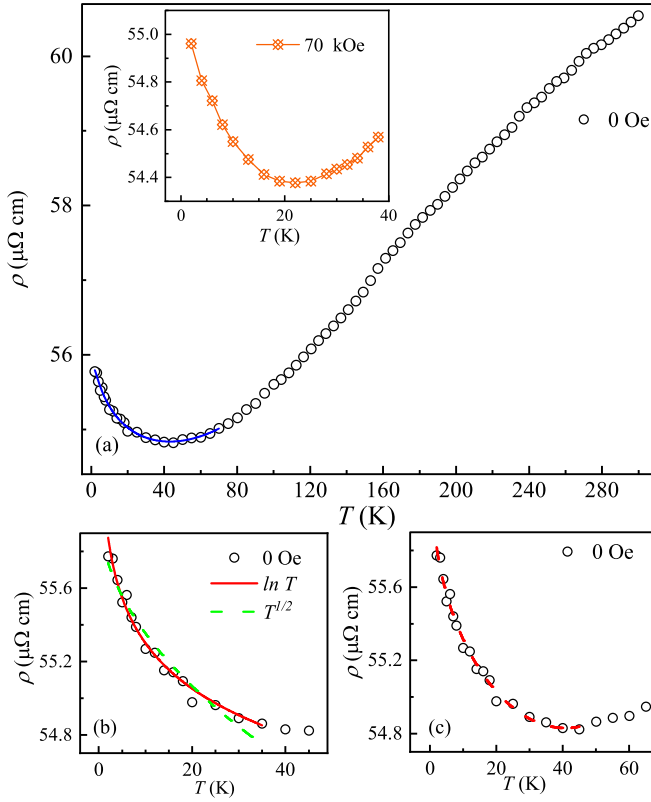


FIG. 5. (a) Temperature dependence of resistivity measured at 0 Oe in the range 2 – 300 K. Blue solid line represents fit to Eq. (8). Inset: Resistivity measured under 70 kOe. (b) Resistivity measured in temperature range 2 – 45 K. (c) Same in the temperature range 2 – 70 K. Dashed red line represents fit to Eq. (9).

a quantum correction term to resistivity, which, manifests as $T^{1/2}$ dependence of ρ for three-dimensional (3D) materials. Also, the resistivity minima do not shift to low temperature on application of H in case of e-e interaction effect. Therefore, to understand the origin of the upturn, low-temperature ρ is fitted with both $\ln T$ and $T^{1/2}$ terms [Fig. 5(b)]. It is noted that the ρ curve is fitted well with $\ln T$, compared to the $T^{1/2}$ term. This suggests the presence of low-temperature Kondo-like effect. Moreover, in several disordered systems, WL is developed due to disorder-induced coherent electron backscattering [55,56]. This yields a $T^{n/2}$ correction term in the ρ (where value of n depends on type of inelastic-scattering process that dominates in given T range) [57]. As there is a presence of site disorder in Ti_2FeAl , the existence of WL effect cannot be ruled out. Therefore, ρ is fitted by combining Kondo-like and WL effect with an equation, given by

$$\rho = \rho_0 + \rho_2 T^2 + \rho_{n/2} T^{-n/2} - \rho_1 \ln T, \quad (8)$$

where ρ_0 corresponds to the residual resistivity and the T^2 term denotes the contributions from delocalized (classical) electron-electron scatterings. The $T^{-n/2}$ term is due to the WL, and the $\ln T$ term corresponds to the Kondo-like effect. A better fit is obtained by considering Eq. (8), as shown by blue solid line in Fig. 5(a). The obtained values of $\rho_{n/2}$, ρ_1 , and n are found to be 9.55×10^{-7} , 5.29×10^{-7} , and $3/4$, respectively. These values indicate that at 0 Oe, a combination

of Kondo-like and WL effect may result in the observed ρ upturn. However, this does not preclude the Kondo-like scattering of conduction electrons. Here, we would also like to mention that the ρ upturn arising solely due to WL effect is generally suppressed by the application of strong H . However, in case of Kondo-like effect the nature of the upturn remains robust, and the T at which minima are observed shifts towards lower T [58]. Further, temperature dependence of ρ is measured under 70 kOe, as shown in inset of Fig. 5(a). It is noted that the nature of the upturn remains unaffected, and minima shift towards lower T . Generally, in conventional ferromagnets, the strength of exchange interactions fixes the direction of spins, and thus, Kondo-like effect is not expected [59]. Therefore, to check whether the increase in ρ at low T is due to Kondo-like behavior, we have considered the modified version of the empirical form of numerical renormalization group (NRG) results given by

$$\rho = \rho_0 [1 + (2^{1/\alpha_s} - 1)(T/T_k)^{\xi_s}]^{-\alpha_s} + \rho_{n/2} T^{-n/2}, \quad (9)$$

where ξ_s and α_s are the fitting parameters and the second term of the equation accounts for the contribution from WL effect. We have fitted our data to the above equation as shown in Fig. 5(c). The data agree well with the NRG results and the values of ξ_s , α_s , and T_k are found to be 1.76 (0.14), 0.049 (0.05), and 2.1 K, respectively. Similar type of result is reported in case of 4.5% Pt-doped $\text{Mn}_{50.5}\text{Bi}_{49.5}$ alloys [60]. Here, we would also like to mention that Pt-doped MnBi is a strong ferromagnet (with Curie temperature above room temperature), where the Kondo-like behavior arises due to the displacement of Mn atoms by nonmagnetic Pt atoms. This results in the weakening of ferromagnetic exchange interaction between Mn spins. These loosely coupled Mn spins give rise to Kondo-like behavior. In case of Ti_2FeAl , as inferred from the structural characterization studies, we have observed A2-type disorder indicating that most likely, all the constituent elements are randomly mixed in the lattice. Hence, when Fe atom can occupy a site surrounded only by nonmagnetic atoms, in this scenario, the loosely coupled Fe atom may certainly be able to behave as a scattering center.

According to some literature reports, an upturn in ρ was also ascribed to e-e interaction and/or weak antilocalization effect [61–63]. However, both these effects result in a positive magnetoresistance. Also, as inferred from ρ curves, Kondo-like effect is not suppressed even at 70 kOe. Therefore, contribution from Kondo effect to magnetoresistance is expected to be negligible. However, in case of WL effect, a negative magnetoresistance is expected since coherent electron backscattering is suppressed by H . Therefore, magnetoresistance (MR, defined as $[(\rho_H - \rho_0)/\rho_0] \times 100\%$) is measured as a function of H at various temperatures [shown in Fig. 6(a)]. Below 30 K, throughout the measured H range, a negative MR is observed. This is also in accordance with magnetization studies, i.e., the system enters an ordered magnetic state below 30 K. This results in suppression of spin disorder scattering leading to negative MR. Further, this clearly rules out the presence of e-e interaction and weak antilocalization effects. As T decreases, the value of MR increases, reaching a maximum at 10 K. However, below 10 K, i.e., in the glassy regime, MR remains constant. This behavior is not unusual

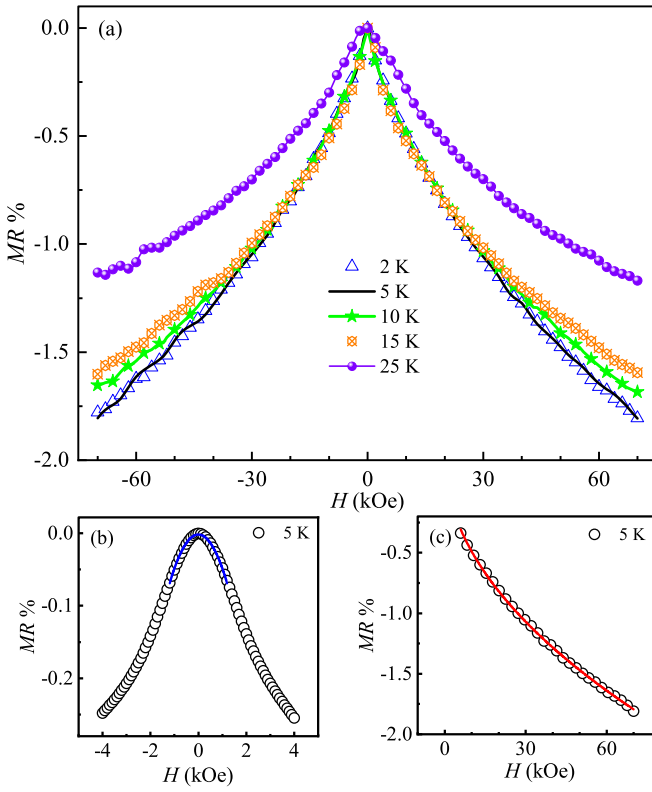


FIG. 6. (a) Magnetoresistance measured at various temperatures in the field range -70 to 70 kOe. Magnetoresistance as a function of H measured at 5 K. (b) In the range -4 to $+4$ kOe. Blue solid line corresponds to H^2 dependence. (c) In the range 5 to 70 kOe. Red solid line corresponds to $H^{1/2}$ dependence.

and has already been reported [64]. Also, in analogy to $M(H)$ curves, the observed MR does not exhibit saturation. For 3D systems, the correction to resistivity due to WL effect scales as H^2 for small magnetic fields and as $H^{1/2}$ for large magnetic fields [65]. Therefore, we have carefully examined the magnetoresistance at 5 K in Ti_2FeAl . For very small fields, the magnetoresistance follows H^2 dependence and then follows a $H^{1/2}$ dependence for large fields as shown in Figs. 6(b) and 6(c). Similar response of magnetoresistance due to WL effect has been observed in other disordered systems [66–68]. This indicates that the negative MR originates from the suppression of WL effect. Therefore, it may be concluded that in case of the arc-furnace cooled Ti_2FeAl alloy, prepared under our synthesis condition, the ρ upturn originates from a combination of Kondo-like behavior and WL effect.

D. Hall resistivity

Several FM alloys exhibit anomalous Hall effect (AHE) originating from the Berry curvature associated with a topologically nontrivial band structure [69,70]. In case of reentrant glassy system, additional contribution to Hall effect may originate from noncollinear magnetic state [71]. Therefore, Hall resistivity (ρ_{xy}) is measured as a function of H . In order to eliminate the contribution from longitudinal resistivity, ρ_{xy} is measured in both positive and negative H directions and has been antisymmetrized using the relation $\rho_{xy} = [\rho_{xy}(+H) -$

$\rho_{xy}(-H)]/2$. Figure 7(a) shows the H dependence of ρ_{xy} at different temperatures in glassy regime. As seen from the figure, with increasing H two distinct humps are noted. This is unusual and the observed nonlinear behavior suggests an unconventional contribution to Hall effect. Further, upon increasing H , ρ_{xy} exhibits a linear behavior up to 50 kOe. This behavior can be attributed to the ordinary Hall effect.

Generally, in case of nonmagnetic systems, ρ_{xy} exhibits a linear magnetic-field dependence. This behavior is also referred to as ordinary Hall effect. However, in case of AHE, ρ_{xy} exhibits similarity with $M(H)$ curves [72]. Further, contributions to AHE can be classified as intrinsic and extrinsic. The intrinsic contribution is generally attributed to spin-orbit coupling, whereas the extrinsic contribution is primarily associated with skew scattering. The extrinsic contribution due to skew scattering usually dominates in case of highly conductive [$\sigma_{xx} > 10^6 (\Omega \text{ cm})^{-1}$] systems and in case of moderately conductive systems [$10^4 < \sigma_{xx} < 10^6 (\Omega \text{ cm})^{-1}$], intrinsic AHE dominates [72,73]. In our case, σ_{xx} is of the order $\sim 2 \times 10^4 (\Omega \text{ cm})^{-1}$. Hence, in case of AHE, the intrinsic contribution is expected to dominate. Therefore, ordinary, and anomalous part of ρ_{xy} can be written as

$$\rho_{xy} = R_0 \mu_0 H + S_H \rho^2 M. \quad (10)$$

Here, R_0 is ordinary Hall coefficient, S_H is a material specific constant, and M is magnetization. However, as seen from Fig. 7(b), at 5 K ρ_{xy} does not follow a path like $M(H)$ indicating a complex behavior. To understand the observed behavior, Eq. (10) is simplified and $\rho_{xy}/\mu_0 H$ is plotted as a function of $\rho^2 M/\mu_0 H$, as shown in Fig. 7(c). In case of AHE, a linear behavior is expected. However, as seen from the figure, the curve does not exhibit linear behavior, indicating that the ordinary and AHE cannot account for the observed feature. This confirms the presence of an unconventional contribution to Hall effect. To quantify the observed unconventional contribution, we have extracted the different contribution to ρ_{xy} at 5 K, as shown in Fig. 7(d). The slope from linear fit of ρ_{xy} at high field is calculated, which is denoted by R_0 . This slope is used to determine the ordinary Hall effect ($R_0 H$), as shown by blue solid line in Fig. 7(d). Also, the anomalous Hall coefficient S_H is determined from slope of $\rho_{xy}/\mu_0 H$ vs $\rho^2 M/\mu_0 H$ curve and the corresponding AHE is calculated using the formula $\rho_{xy}^{\text{AHE}} = S_H \rho^2 M$, where ρ is resistivity and M is magnetization. Finally, we have subtracted the calculated ordinary and anomalous contribution from the observed ρ_{xy} to obtain the unconventional contribution (ρ_{xy}^{UAHE}), i.e.,

$$\rho_{xy}^{\text{UAHE}} = \rho_{xy} - (R_0 \mu_0 H + S_H \rho^2 M). \quad (11)$$

Similarly, the different contributions to ρ_{xy} at 2 K are also extracted using the same procedure (not shown). The unconventional contribution at 2 and 5 K are found to be ~ 20 and $14 \mu\Omega \text{ cm}$, respectively. It is well known that in systems hosting noncoplanar spin textures such as skyrmions, an additional contribution to Hall effect is observed which is referred to as topological Hall effect [74–76]. However, this configuration usually gives rise to a unique feature in H dependence of ac magnetization [77]. This feature is absent in our system, indicating that the crystallization of skyrmions is highly unlikely. Therefore, in Ti_2FeAl , the observed unconventional

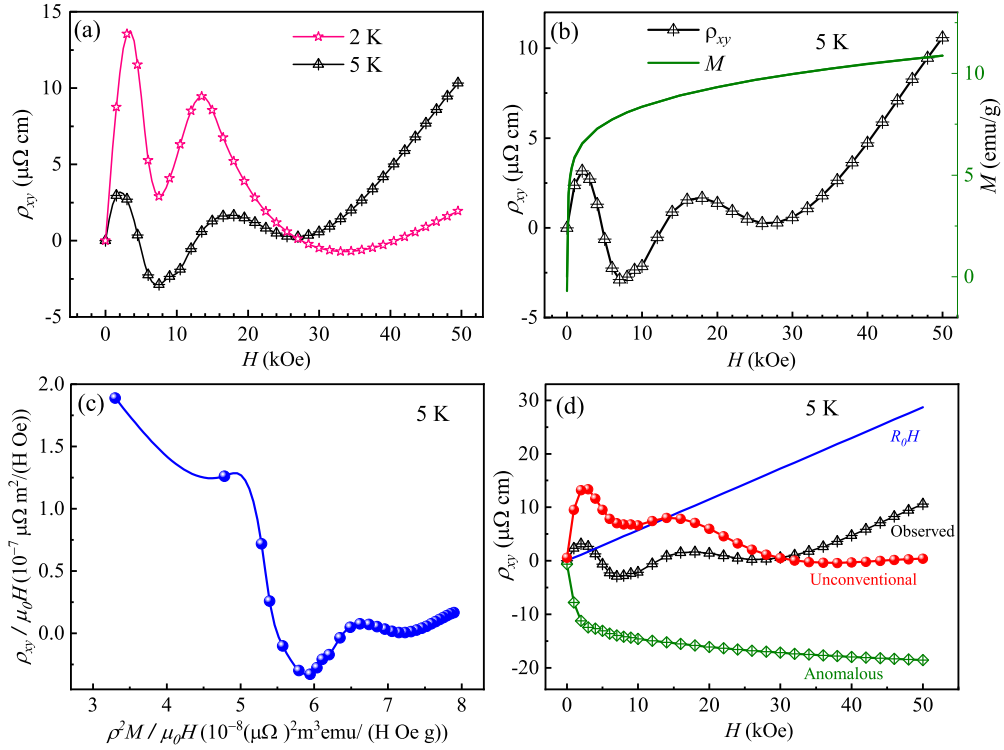


FIG. 7. (a) Hall resistivity measured at different temperatures in the range 0–50 kOe. (b) Left axis: Hall resistivity measured at 5 K, in the range 0–50 kOe. Right axis: Magnetization measured at 5 K, as a function of H in the range 0–50 kOe. (c) Plot of $\rho_{xy}/\mu_0 H$ vs $\rho^2 M/\mu_0 H$ in the range 0–50 kOe at 5 K. (d) Extracted components of Hall resistivity at 5 K in the range 0–50 kOe.

contribution to Hall effect originates from noncollinear spin state in the reentrant CG regime.

IV. DISCUSSION

In case of Ti_2FeAl (under our synthesis protocol), as inferred from the structural characterization studies, A2-type disorder results in random mixing of Ti, Fe, and Al in the crystal lattice. This indicates that even though Ti_2FeAl system has been considered as an inverse Heusler alloy theoretically, in our case such ordering is not favored. Instead, this system adopts a fully disordered bcc structure. Here, we would also like to mention that in case of binary $\text{Ti}_{50}\text{Fe}_{50}$ alloy with CsCl ($B2$ -type) structure, Fe can be substituted by Al (around 42%) without affecting the $B2$ order. The A2-disordered βTi becomes ordered $B2$ by substitution of Ti by Fe and Al [27]. However, presence of $B2$ -like correlations is valid only if the ternary Ti-Fe-Al system has traces of such phases. Therefore, in our case, it is reasonable to assume that when crystallographically averaged, the chemical disorder results in a random mixing of constituent elements, which can be visualized as distribution of magnetic Fe atoms in a nonmagnetic matrix of Ti and Al atoms. Here, the nature of exchange interaction is of RKKY type, which oscillates in sign depending upon the distance between nearest Fe atoms. Therefore, disorder in our system may create a complex distribution of ferro- and antiferromagnetic exchange interactions, which may result in glassy dynamics at low temperatures.

Wasserman *et al.* [78] studied the magnetic properties of $\text{Ti}_{50}\text{Fe}_{50}$ and reported the presence of superparamagnetic clusters, which was attributed to Fe-rich regions arising due to

incomplete chemical ordering. Notably, they also observed the presence of Fe-Fe FM exchange interactions leading to a deviation from CW law above 225 K [78]. Additionally, it is interesting to note that the stoichiometric $L2_1$ -ordered Fe_2AlTi exhibits a FM ordering around $T_C \sim 123$ K [79]. Also, in C14 Laves phase of $(\text{Fe}_{1-x}\text{Al}_x)_2\text{Ti}$ with $x \leq 0.5$, the antiferromagnetism in Fe_2Ti is suppressed with addition of Al [80]. However, in this case the lattice is hexagonal, and the local Fe environment is different from bcc lattice. All these scenarios indicate the importance of local Fe environment in determining the nature and strength of Fe-Fe exchange interactions. In our case, from dc and ac magnetization studies it is noted that Ti_2FeAl undergoes a FM ordering around 30 K, followed by a transition to CG state below 10 K. This behavior is referred to as reentrant cluster glass state. Such features were also observed in a few Mn-Ni based Heusler alloys where it was attributed to random occupation of lattice sites by Mn atoms [81,82]. Also, in Heusler alloys with general formula Z_2YX such as Ga_2MnCo and Al_2MnCo , RSG behavior was observed which was attributed to the unit-cell expansion at the transition temperature and to competing FM and AFM interactions, respectively [37,83]. However, in our case of Ti_2FeAl the randomness results in the emergence of a reentrant CG state. Further, in case of RSG systems, the disorder can also give rise to a noncollinear spin state. This noncollinearity results in the nonsaturation of magnetization even under an applied field of 70 kOe, as observed from magnetic isotherm curves. Here, we would like to mention that extremely high value of magnetocrystalline anisotropy also gives rise to nonsaturation. However, this should be reflected in observation of a large coercivity, which is absent

in our system. Additionally, as noted from resistivity studies, an upturn is observed below 40 K, which mimics Kondo-like behavior along with WL. Generally, in conventional ferromagnets, Kondo-like behavior is not expected since direction of the spins is fixed by the exchange interactions. However, in our case, the A2-type disorder may result in weakening the strength of exchange interactions. This indicates that some Fe spins will be coupled strongly whereas some will be coupled weakly. The loosely coupled spins may undergo Kondo-like scattering to give rise to the observed resistivity upturn. Also, at low T , a negative MR is noted which follows H^2 dependence for very small fields and then follows a $H^{1/2}$ dependence for large fields. The observed behavior suggests the existence of WL effect. Further, an exciting result is obtained in Hall resistivity measurements, where a large unconventional contribution is observed. In case of glassy magnetic systems, the origin of anomalous Hall effect is attributed to the presence of a frustrated noncoplanar spin structure [84–86], whereas in case of FM materials, the Hall resistivity follows a path similar to $M(H)$ curve. However, in Ti_2FeAl this is not the case, which points toward a complex magnetic landscape at low T . Nevertheless, the large unconventional contribution to Hall resistivity confirms the presence of a noncollinear spin state in Ti_2FeAl . Therefore, we believe that Ti_2FeAl is an important bcc alloy due to its richness in terms of the observed physical phenomena and to understand

the role of disorders in determining the physical properties of such alloys.

V. CONCLUSION

To conclude, Ti_2FeAl , when prepared under our synthesis protocol, crystallizes in a body-centered cubic structure with significant structural disorder rather than the theoretically predicted XA structure. This results in randomly placed Fe atoms in the lattice giving rise to a complex magnetic ground state. Systematic analysis of dc and ac magnetization reveals that this alloy undergoes a FM ordering around 30 K followed by a reentrant cluster glass state below 10 K. The anomaly noted in the ρ curve, and the MR behavior are ascribed to coexistence of Kondo-like behavior and weak localization effect. Interestingly, in Hall resistivity, an unconventional contribution is noted which arises due to the presence of a noncollinear state in the reentrant CG regime. Hence, we believe that our studies may open a route to understand the role of site disorder in development of reentrant CG state and unconventional electrical transport properties in such alloys.

ACKNOWLEDGMENT

The authors acknowledge IIT Mandi for experimental facilities and financial support.

-
- [1] K. Binder, A. P. Young, and C. D. F. Gen, Spin glasses: Experimental facts, theoretical concepts, and open questions, *Rev. Mod. Phys.* **58**, 801 (1986).
 - [2] S. Blundell, *Magnetism in Condensed Matter* (Oxford University Press, Oxford, 2001).
 - [3] G. Yu, H. Chen, S. Ma, X. Luo, C. Liu, C. Chen, C. Fang, Y. Yuan, X. Ye, and Z. Zhong, Robust topological Hall effect in a reentrant spin glass system $\text{Mn}_{1.89}\text{Pt}_{0.98}\text{Ga}_{1.12}$, *Physica B: Condens. Matter* **640**, 414043 (2022).
 - [4] F. Heusler, The nature of Heusler alloys, *Trans. Faraday Soc.* **8**, 169 (1912).
 - [5] T. Graf, C. Felser, and S. S. P. Parkin, Simple rules for the understanding of Heusler compounds, *Prog. Solid State Chem.* **39**, 1 (2011).
 - [6] K. Yadav and K. Mukherjee, Evidence of multi-band superconductivity in non-centrosymmetric full Heusler alloy LuPd_2Sn , *J. Phys.: Condens. Matter* **35**, 275601 (2023).
 - [7] I. Galanakis, P. H. Dederichs, and N. Papanikolaou, Slater-Pauling behavior and origin of the half-metallicity of the full-Heusler alloys, *Phys. Rev. B* **66**, 174429 (2002).
 - [8] S. Chadov, X. Qi, J. Kübler, G. H. Fecher, C. Felser, and S. C. Zhang, Tunable multifunctional topological insulators in ternary Heusler compounds, *Nat. Mater.* **9**, 541 (2010).
 - [9] C. Schindler, S. Galeski, W. Schnelle, R. Wawrzyńczak, W. Abdel-Haq, S. N. Guin, J. Kroder, N. Kumar, C. Fu, H. Borrmann, C. Shekhar, C. Felser, T. Meng, A. G. Grushin, Y. Zhang, Y. Sun, and J. Gooth, Anisotropic electrical and thermal magnetotransport in the magnetic semimetal GdPtBi , *Phys. Rev. B* **101**, 125119 (2020).
 - [10] A. Laha, S. Malick, R. Singha, P. Mandal, P. Rambabu, V. Kanchana, and Z. Hossain, Magnetotransport properties of the correlated topological nodal-line semimetal YbCdGe , *Phys. Rev. B* **99**, 241102(R) (2019).
 - [11] C. Phatak, O. Heinonen, M. De Graef, and A. Petford-Long, Nanoscale skyrmions in a nonchiral metallic Multiferroic: Ni_2MnGa , *Nano Lett.* **16**, 4141 (2016).
 - [12] A. K. Nayak, V. Kumar, T. Ma, P. Werner, E. Pippel, R. Sahoo, F. Damay, U. K. Röbler, C. Felser, and S. S. P. Parkin, Magnetic antiskyrmions above room temperature in tetragonal Heusler materials, *Nature (London)* **548**, 561 (2017).
 - [13] S. Chakraborty, S. Gupta, and C. Mazumdar, Rare coexistence of disorder-induced griffiths phase and reentrant spin-glass state in a heusler alloy Rh_2FeAl with high Curie temperature, *J. Alloys Compd.* **976**, 173215 (2024).
 - [14] G. K. Shukla *et al.*, Atomic disorder and Berry phase driven anomalous Hall effect in a Co_2FeAl Heusler compound, *Phys. Rev. B* **105**, 035124 (2022).
 - [15] Z. Dong *et al.*, High-performance non-Fermi-liquid metallic thermoelectric materials, *npj Comput. Mater.* **9**, 41 (2023).
 - [16] D. Rani, J. Kangsabanik, K. G. Suresh, N. Patra, D. Bhattacharyya, S. N. Jha, and A. Alam, Origin of local atomic order and disorder in $\text{Co}_2\text{Fe}_{1-x}\text{Cr}_x\text{Si}$ Heusler alloys: Theory and experiment, *Phys. Rev. Appl.* **10**, 054022 (2018).
 - [17] Q. L. Fang, J. M. Zhang, and K. W. Xu, Magnetic properties and origin of the half-metallicity of Ti_2MnZ ($Z = \text{Al, Ga, In, Si, Ge, Sn}$) Heusler alloys with the Hg_2CuTi -type structure, *J. Magn. Magn. Mater.* **349**, 104 (2014).
 - [18] L. Zhang, X. T. Wang, H. Rozale, J. Lu, and L. Wang, Half-metallicity and tetragonal deformation of Ti_2RhAl , Ti_2RhGa ,

- and Ti_2RhIn : A first-principle study, *J. Supercond. Nov. Magn.* **29**, 349 (2016).
- [19] X. P. Wei, J. B. Deng, G. Y. Mao, S. Bin Chu, and X. R. Hu, Half-metallic properties for the Ti_2YZ ($Y = \text{Fe}, \text{Co}, \text{Ni}$, $Z = \text{Al}, \text{Ga}, \text{In}$) Heusler Alloys: A first-principles study, *Intermetallics* **29**, 86 (2012).
- [20] K. Özdoğan and I. Galanakis, Stability of spin-gapless semi-conducting behavior in Ti_2CoSi , Ti_2MnAl , and Ti_2VAs Heusler compounds, *Phys. Rev. Mater.* **5**, 024409 (2021).
- [21] Q.-L. Fang, J.-M. Zhang, K.-W. Xu, and V. Ji, The effect of defects on the magnetic properties and spin polarization of Ti_2FeAl Heusler alloy, *J. Magn. Magn. Mater.* **351**, 25 (2014).
- [22] F. Dahmane, S. Benalia, L. Djoudi, A. Tadjer, R. Khenata, B. Doumi, and H. Aourag, First-principles study of structural, electronic, magnetic and half-metallic properties of the heusler alloys Ti_2ZAl ($Z = \text{Co}, \text{Fe}, \text{Mn}$), *J. Supercond. Nov. Magn.* **28**, 3099 (2015).
- [23] M. Drief, Y. Guermit, N. Benkhetto, D. Rached, H. Rached, and T. Lantri, First-principle study of half-metallic ferrimagnet behavior in titanium-based Heusler alloys Ti_2FeZ ($Z = \text{Al}, \text{Ga}, \text{and In}$), *J. Supercond. Nov. Magn.* **31**, 1059 (2018).
- [24] X. J. Zhang, Z. H. Liu, Y. J. Zhang, H. Y. Liu, G. D. Liu, Y. T. Cui, and X. Q. Ma, Theoretical and experimental study of the phase formation for Ti_2YAl and $\text{Ti}_2\text{Y}'\text{Ga}$ ($Y = \text{Co}, \text{Fe}$; $Y' = \text{Cr}, \text{Fe}$), *Intermetallics* **73**, 26 (2016).
- [25] J. Goraus and J. Czerniewski, Magnetic properties of Ti_2MnAl , Ti_2FeAl and Ti_2FeGa compounds, *J. Magn. Magn. Mater.* **498**, 166106 (2020).
- [26] K. M. Law, R. Nahar, R. Nold, M. Zengel, J. Lewis, and A. J. Hauser, Phase and D-d hybridization control via electron count for material property control in the X_2FeAl material class, *J. Magn. Magn. Mater.* **596**, 171932 (2024).
- [27] M. Palm and J. Lacaze, Assessment of the Al-Fe-Ti system, *Intermetallics* **14**, 1291 (2006).
- [28] H. M. Rietveld, The Rietveld method, *Phys. Scr.* **89**, 098002 (2014).
- [29] M. Singh, H. S. Saini, J. Thakur, A. H. Reshak, and M. K. Kashyap, Disorder dependent half-metallicity in Mn_2CoSi inverse Heusler alloy, *J. Solid State Chem.* **208**, 71 (2013).
- [30] K. Momma and F. Izumi, VESTA 3 for three-dimensional visualization of crystal, volumetric and morphology data, *J. Appl. Crystallogr.* **44**, 1272 (2011).
- [31] J. A. Mydosh, Spin glasses: Redux: An updated experimental/materials survey, *Rep. Prog. Phys.* **78**, 052501 (2015).
- [32] M. K. Sharma, K. Yadav, and K. Mukherjee, Complex magnetic behaviour and evidence of a superspin glass state in the binary intermetallic compound Er_5Pd_2 , *J. Phys.: Condens. Matter* **30**, 215803 (2018).
- [33] K. Yadav, M. K. Sharma, S. Singh, and K. Mukherjee, Exotic magnetic behaviour and evidence of cluster glass and Griffiths like phase in Heusler alloys $\text{Fe}_{2-x}\text{Mn}_x\text{CrAl}$ ($0 \leq x \leq 1$), *Sci. Rep.* **9**, 15888 (2019).
- [34] G. Kaur and K. Mukherjee, Emergence of low-temperature glassy dynamics in Ru substituted non-magnetic insulator CaHfO_3 , *J. Phys.: Condens. Matter* **34**, 415802 (2022).
- [35] D. Ranaut, M. Rani, and K. Mukherjee, Nonequilibrium dynamics and discretization of energy levels in the inverse spinel LiCoVO_4 , *Phys. Rev. B* **107**, 214413 (2023).
- [36] V. K. Anand, D. T. Adroja, and A. D. Hillier, Ferromagnetic cluster spin-glass behavior in PrRhSn_3 , *Phys. Rev. B* **85**, 014418 (2012).
- [37] T. Samanta, P. A. Bhoje, A. Das, A. Kumar, and A. K. Nigam, Reentrant cluster glass and stability of ferromagnetism in the Ga_2MnCo Heusler alloy, *Phys. Rev. B* **97**, 184421 (2018).
- [38] J. F. Malta, M. S. Marta, J. A. Paixão, and A. P. Gonçalves, Evidence of a cluster spin-glass phase in the skyrmion-hosting GaMo_4S_8 compound, *J. Mater. Chem. C Mater.* **10**, 12043 (2022).
- [39] J. L. Tholence, On the frequency dependence of the transition temperature in spin glasses, *Solid State Commun.* **35**, 113 (1980).
- [40] See Supplemental Material at <http://link.aps.org/supplemental/10.1103/PhysRevB.110.054433> for information about the characterization of the cluster glass state by magnetic relaxation and memory effect measurements along with heat capacity studies.
- [41] R. V. Chamberlin, G. Mozurkewich, and R. Orbach, Time decay of the remanent magnetization in spin-glasses, *Phys. Rev. Lett.* **52**, 867 (1984).
- [42] K. Mukherjee, K. Kumar, A. Banerjee, and P. Chaddah, On the correlation between supercooling, superheating and kinetic arrest in a magnetic glass $\text{Pr}_{0.5}\text{Ca}_{0.5}\text{Mn}_{0.975}\text{Al}_{0.025}\text{O}_3$, *Eur. Phys. J. B* **86**, 21 (2013).
- [43] S. Pakhira, C. Mazumdar, R. Ranganathan, S. Giri, and M. Avdeev, Large magnetic cooling power involving frustrated antiferromagnetic spin-glass state in R_2NiSi_3 ($\text{R} = \text{Gd}, \text{Er}$), *Phys. Rev. B* **94**, 104414 (2016).
- [44] P. Bag, P. R. Baral, and R. Nath, Cluster spin-glass behavior and memory effect in $\text{Cr}_{0.5}\text{Fe}_{0.5}\text{Ga}$, *Phys. Rev. B* **98**, 144436 (2018).
- [45] J. O. Thomson and J. R. Thompson, Low-temperature excitations in spin glasses: Evidence for a $T^{3/2}$ behaviour, *J. Phys. F: Met. Phys.* **11**, 247 (1981).
- [46] S. Kustov, J. Torrens-Serra, E. K. H. Salje, and D. N. Beshers, Re-entrant spin glass transitions: New insights from acoustic absorption by domain walls, *Sci. Rep.* **7**, 16846 (2017).
- [47] S. Chatterjee, S. Giri, S. K. De, and S. Majumdar, Reentrant spin-glass state $\text{Ni}_2\text{Mn}_{1.36}\text{Sn}_{0.64}$ shape-memory alloy, *Phys. Rev. B* **79**, 092410 (2009).
- [48] M. Nielsen, D. Ryan, H. Guo, and M. Zuckermann, Magnetic ordering in the three-dimensional site-disordered Heisenberg model, *Phys. Rev. B* **53**, 343 (1996).
- [49] W. M. Saslow and G. Parker, "Melting" of frustrated spins: Mechanism for reentrant ferromagnetic-spin-glass behavior, *Phys. Rev. Lett.* **56**, 1074 (1986).
- [50] L. A. Longchar, M. Rahaman, B. Krishna Hazra, R. Rawat, M. Manivel Raja, S. N. Kaul, and S. Srinath, Resistivity minima in disordered $\text{Co}_2\text{FeAl}_{0.5}\text{Si}_{0.5}$ Heusler alloy thin films, *J. Magn. Magn. Mater.* **569**, 170439 (2023).
- [51] B. Venkateswarlu, P. V. Midhunlal, P. D. Babu, and N. H. Kumar, Magnetic and anomalous electronic transport properties of the quaternary Heusler alloys $\text{Co}_2\text{Ti}_{1-x}\text{Fe}_x\text{Ge}$, *J. Magn. Magn. Mater.* **407**, 142 (2016).
- [52] K. H. J. Buschow and H. J. Van Daal, Evidence for the presence of the Kondo effect in the compound CeAl_2 , *Phys. Rev. Lett.* **23**, 408 (1969).
- [53] W. Niu, M. Gao, X. Wang, F. Song, J. Du, X. Wang, Y. Xu, and R. Zhang, Evidence of weak localization in quantum interference effects observed in epitaxial $\text{La}_{0.7}\text{Sr}_{0.3}\text{MnO}_3$ ultrathin films, *Sci. Rep.* **6**, 26081 (2016).

- [54] D. Kumar, J. Sankar, J. Narayan, R. K. Singh, and A. K. Majumdar, Low-temperature resistivity minima in colossal magnetoresistive $\text{La}_{0.7}\text{Ca}_{0.3}\text{MnO}_3$ thin films, *Phys. Rev. B* **65**, 094407 (2002).
- [55] M. Aftab, G. Hassnain Jaffari, S. K. Hasanain, T. A. Abbas, and S. Ismat Shah, Disorder and weak localization effects in $\text{Co}_2\text{Mn}_x\text{Ti}_{1-x}\text{Al}$ Heusler alloy thin films, *J. Phys. D: Appl. Phys.* **45**, 475001 (2012).
- [56] S. Biswas, S. Islam, N. S. Kander, and A. K. Das, Growth, magnetic, transport and electronic properties of Co_2TiSi Heusler alloy thin films, *J. Alloys Compd.* **968**, 171980 (2023).
- [57] P. A. Lee and T. V. Ramakrishnan, Disordered electronic systems, *Rev. Mod. Phys.* **57**, 287 (1985).
- [58] S. Ghosh, R. G. Tanguturi, P. Pramanik, D. C. Joshi, P. K. Mishra, S. Das, and S. Thota, Low-temperature anomalous spin correlations and Kondo effect in ferromagnetic $\text{SrRuO}_3/\text{LaNiO}_3/\text{La}_{0.7}\text{Sr}_{0.3}\text{MnO}_3$ trilayers, *Phys. Rev. B* **99**, 115135 (2019).
- [59] K. R. Sapkota, F. S. Maloney, and W. Wang, Observations of the Kondo effect and its coexistence with ferromagnetism in a magnetically undoped metal oxide nanostructure, *Phys. Rev. B* **97**, 144425 (2018).
- [60] P. Kharel, R. Skomski, P. Lukashev, R. Sabirianov, and D. J. Sellmyer, Spin correlations and Kondo effect in a strong ferromagnet, *Phys. Rev. B* **84**, 014431 (2011).
- [61] D. Gnida, K. Ciesielski, and D. Kaczorowski, Origin of the negative temperature coefficient of resistivity in the half-Heusler antimonides LuNiSb and YPdSb , *Phys. Rev. B* **103**, 174206 (2021).
- [62] R. Pang, J. Tian, C. Kang, L. Wang, H. Gu, M. Shen, L. She, Y. Song, X. Liu, and W. Zhang, Low-temperature resistivity upturn and weak antilocalization in layered $\text{Ta}_{1.04}\text{Ru}_{0.78}\text{Te}_4$ bulk single crystal, *Appl. Phys. Lett.* **123**, 051907 (2023).
- [63] P. Kumar, V. Nagpal, Sudesh, and S. Patnaik, Chiral anomaly induced negative magnetoresistance and weak anti-localization in Weyl semimetal $\text{Bi}_{0.97}\text{Sb}_{0.03}$ alloy, *J. Phys.: Condens. Matter* **34**, 055601 (2022).
- [64] K. Yadav, P. Koushik, S. Singh, M. Hagihala, and K. Mukherjee, Existence of complex magnetic ground state and topological Hall effect in centrosymmetric silicide DyScSi , *New J. Phys.* **25**, 123030 (2023).
- [65] E. M. Likovich, K. J. Russell, E. W. Petersen, and V. Narayanamurti, Weak localization and mobility in ZnO nanostructures, *Phys. Rev. B* **80**, 245318 (2009).
- [66] J. M. Moya, C.-L. Huang, J. Choe, G. Costin, M. S. Foster, and E. Morosan, Effect of synthesis conditions on the electrical resistivity TiSe_2 , *Phys. Rev. Mater.* **3**, 084005 (2019).
- [67] L. M. B. Vargas, K. Bolaños, M. J. da Silva, S. de Castro, M. L. Peres, and M. P. F. de Godoy, Weak localization effect in $\text{Zn}_{1-x}\text{Cd}_x\text{O}/\text{CdO}$ heterostructures, *J. Appl. Phys.* **133**, 025701 (2023).
- [68] J. Mukherjee and M. S. Ramachandra Rao, Localization crossover and phase coherent electron transport in a-InGaZnO_4 thin films, *Appl. Phys. Lett.* **110**, 122101 (2017).
- [69] G. K. Shukla, J. Sau, N. Shahi, A. K. Singh, M. Kumar, and S. Singh, Anomalous Hall effect from gapped nodal line in the Co_2FeGe Heusler compound, *Phys. Rev. B* **104**, 195108 (2021).
- [70] S. Roy, R. Singha, A. Ghosh, A. Pariari, and P. Mandal, Anomalous Hall effect in the half-metallic Heusler compound Co_2TiX ($X = \text{Si, Ge}$), *Phys. Rev. B* **102**, 085147 (2020).
- [71] C. Sürgers, G. Fischer, P. Winkel, and H. V. Löhneysen, Large topological Hall effect in the non-collinear phase of an antiferromagnet, *Nat. Commun.* **5**, 3400 (2014).
- [72] N. Nagaosa, J. Sinova, S. Onoda, A. H. MacDonald, and N. P. Ong, Anomalous Hall effect, *Rev. Mod. Phys.* **82**, 1539 (2010).
- [73] S. Friedemann, M. Brando, W. J. Duncan, A. Neubauer, C. Pfleiderer, and F. M. Grosche, Ordinary and intrinsic anomalous Hall effects in $\text{Nb}_{1-y}\text{Fe}_{2+y}$, *Phys. Rev. B* **87**, 024410 (2013).
- [74] T. Kurumaji, T. Nakajima, M. Hirschberger, A. Kikkawa, Y. Yamasaki, H. Sagayama, H. Nakao, Y. Taguchi, T. -Hisa Arima, and Y. Tokura, Skyrmion lattice with a giant topological Hall effect in a frustrated triangular-lattice magnet, *Science* **365**, 914 (2019).
- [75] D. Liang, J. P. DeGrave, M. J. Stolt, Y. Tokura, and S. Jin, Current-driven dynamics of skyrmions stabilized in MnSi nanowires revealed by topological Hall effect, *Nat. Commun.* **6**, 8217 (2015).
- [76] N. Kanazawa, M. Kubota, A. Tsukazaki, Y. Kozuka, K. S. Takahashi, M. Kawasaki, M. Ichikawa, F. Kagawa, and Y. Tokura, Discretized topological Hall effect emerging from skyrmions in constricted geometry, *Phys. Rev. B* **91**, 041122(R) (2015).
- [77] A. Bauer and C. Pfleiderer, Magnetic phase diagram of MnSi inferred from magnetization and ac susceptibility, *Phys. Rev. B* **85**, 214418 (2012).
- [78] E. F. Wassermann, B. Rellinghaus, Th. Roessel, and W. Pepperhoff, Relation between structure and magnetism of $\text{Ti}_x\text{Fe}_{100-x}$ alloys within the C14 Laves-phase stability range, *J. Magn. Magn. Mater.* **190**, 289 (1998).
- [79] K. H. J. Buschow and P. G. van Engen, Magnetic and magneto-optical properties of Heusler alloys based on aluminium and gallium, *J. Magn. Magn. Mater.* **25**, 90 (1981).
- [80] Y. Yamada, K. Kuroda, K. Matono, and A. Sakata, Magnetisation and NMR studies of magnetic properties of $\text{Ti}(\text{Fe}_{1-x}\text{Al}_x)_2$, *J. Phys. Soc. Jpn.* **69**, 225 (2000).
- [81] L. Ma, W. H. Wang, J. B. Lu, J. Q. Li, C. M. Zhen, D. L. Hou, and G. H. Wu, Coexistence of reentrant-spin-glass and ferromagnetic martensitic phases in the $\text{Mn}_2\text{Ni}_{1.6}\text{Sn}_{0.4}$ Heusler alloy, *Appl. Phys. Lett.* **99**, 182507 (2011).
- [82] M. Khan and A. Albagami, Cooling field dependent exchange bias in $\text{Mn}_2\text{Ni}_{1.4}\text{Ga}_{0.6}$: A reentrant spin glass system with short range ferromagnetic ordering, *J. Alloys Compd.* **727**, 100 (2017).
- [83] H. Shiraishi, T. Hori, and Y. Yamaguchi, Magnetic properties of pseudo-binary $\text{GaCo}_{1-x}\text{Cr}_x$ and $\text{AlCo}_{1-x}\text{Mn}_x$ ($M = \text{Fe, Mn}$) systems, *J. Magn. Magn. Mater.* **104–107**, 2040 (1992).
- [84] J. Kroder *et al.*, Spin glass behavior in the disordered half-Heusler compound IrMnGa , *Phys. Rev. B* **99**, 174410 (2019).
- [85] T. Taniguchi, K. Yamanaka, H. Sumioka, T. Yamazaki, Y. Tabata, and S. Kawarazaki, Direct observation of chiral susceptibility in the canonical spin glass AuFe , *Phys. Rev. Lett.* **93**, 246605 (2004).
- [86] P. Pureur, F. W. Fabris, J. Schaf, and I. A. Campbell, Chiral susceptibility in canonical spin glass and re-entrant alloys from Hall effect measurements, *Europhysics Letters (EPL)* **67**, 123 (2004).